

Data Mining and Machine Learning Methods Applied to 3 A Numerical Clinching Model

Marco Götz^{1,*}, Ferenc Leichsenring¹, Thomas Kropp², Peter Müller², Tobias Falk²,
Wolfgang Graf¹, Michael Kaliske¹ and Welf-Guntram Drossel²

Abstract: Numerical mechanical models used for design of structures and processes are very complex and high-dimensionally parametrised. The understanding of the model characteristics is of interest for engineering tasks and subsequently for an efficient design. Multiple analysis methods are known and available to gain insight into existing models. In this contribution, selected methods from various fields are applied to a real world mechanical engineering example of a currently developed clinching process. The selection of introduced methods comprises techniques of machine learning and data mining, in which the utilization is aiming at a decreased numerical effort. The methods of choice are basically discussed and references are given as well as challenges in the context of meta-modelling and sensitivities are shown. An incremental knowledge gain is provided by a step-by-step application of the numerical methods, whereas resulting consequences for further applications are highlighted. Furthermore, a visualisation method aiming at an easy design guideline is proposed. These visual decision maps incorporate the uncertainty coming from the reduction of dimensionality and can be applied in early stage of design.

Keywords: Design, data mining, computational intelligence, meta-modelling, permissible design space, sensitivity analysis, self-organizing maps, inverse problem, early stage of design, clinching.

Notation

ξ	deterministic simulation model
ξ^*	meta-model of the deterministic simulation model
\square	vector-valued quantity
\mathbf{X}	space of input parameter
\mathcal{X}	set of input vectors
x	input quantity

¹Institute for Structural Analysis, Technische Universität, Dresden, Germany.

²Fraunhofer Institute for Machine Tools and Forming Technology, Dresden, Germany.

* Corresponding Author: Marco Götz. Email: marco.goetz@tu-dresden.de.

n_x	number of input quantities, with counter variable i
\mathbf{Z}	space of result parameter
\mathcal{Z}	set of result of result vectors
z	result quantity
n_z	number of result quantities, with counter variable j
n_{sim}	number of deterministic simulations, with counter variable l
\square_{perm}	indicator of permissibility
\square_{nperm}	indicator of non-permissibility
\square	empirical mean value
$S_{x_i z_j}^{\square}$	sensitivity of input parameter x_i with respect to result quantity z_j

1 Introduction

The ongoing digitalisation includes significant changes in the design of structures and processes. Due to high costs the design of new products or production processes by ‘trial-and-error’ investigations at real prototypes seems not economically justifiable any more. To overcome this, a simulation-based design process is established in many industries. The main idea is to simulate the new product/process by a numerical model. In general, this model is parametrised with n_x input parameters x_i in order to find a suitable set of parameters fulfilling constraints and optimality criteria. The challenging task is, to parametrise the model and to identify the optimal design. For supporting this process many numerical tools are available and need to be applied specifically. The main goals for these methods are: Gaining **insight** into the numerical simulation model, identifying **influences** of the parameters to constraints and optimality criteria and **support** the design process in an **efficient** manner. In the context of ‘computational intelligence’, the applied methods/tools are mainly associated with two research areas: **Data mining** and **machine learning**. These fields are highly innovative and the application possibilities of ‘big data’-methods are enormous. In contrast to the application field ‘big data’, the engineering tasks are characterized by ‘small data’, because the generation of data (i.e. multiple simulation model computations) is highly expensive.

Therefore, the common procedure in a simulation-based design process is as follows:

1. development and parametrisation of a simulation model,
2. computing a sample set (Design of Experiments),
3. explore the sample set by data mining methods,
4. construct a meta-model with machine learning methods,
5. use the meta-model for:
 - (a) sensitivity analysis,

- (b) uncertainty analysis,
- (c) optimisation.

Many modifications or exchanges in this order of steps are possible, e.g. occasionally iterative improvements are necessary. The common guiding theme of this contribution is to discuss and apply several methods at a real design task in the context of a clinching process. The requirements for the design of mechanical joints have increased steadily in recent years. In the past, the main requirements that have significantly influenced the development of mechanical joining technology were economic efficiency, productivity, process reliability and lightweight construction. A common technology for joining sheet metal is clinching. When using clinching, the sheet metal is locally formed, a ductile material is required but no rivet or any other further element is needed and no heat is induced into the joining zone. Currently, clinching is used only for thin sheet metal, because the determination of the tool geometry parameters is done by empirical knowledge in combination with experimental tests. Unfortunately, the suitability of clinching for connecting substantially longer sheet metal thickness has neither been sufficiently investigated and suitable toolkits for larger overall sheet metal thickness are only available in very small quantities and only in a few sizes. The state-of-the-art for ascertaining tools for larger sheet metal thickness and point dimensions is trial-and-error, which leads to high costs caused by producing a large number of tools and doing experiments. This paper demonstrates some analytical approaches to this problem in order to obtain a suitable tool design for clinching thick sheet metal with the help of a finite element analysis in combination with machine learning methods. The clinching model is introduced in Section 2. The applied methods are well established and only briefly reviewed. The exploration of existing data by data mining methods is discussed in Section 3. In order to increase the efficiency, two different types of meta-models are compared in Section 4 and utilized for the sensitivity evaluation in Section 5. Furthermore, a new method for simplification of the design process is proposed, see Section 6. Therefore, two-dimensional nomographs are developed, which are common visual aids in engineering related design tasks. On the basis of the acquired information about the simulation model, ‘decision maps’ are constructed. A list of the most relevant symbols can be found at the end of this paper.

1.1 Simulation model

As described, the foundation of simulation-based design is a parametrised simulation model. Examples for simulation models are analytical functions or finite element models. The parametrisation of the model is done by n_x input parameters assembled in an input vector \underline{x} (also called feature vector). The related input space $\mathbf{X} \subset \mathbb{R}^{n_x}$ is usually composed of restricted intervals for each dimension

$$\mathbf{X} = I_1 \times I_2 \times \dots \times I_i \times \dots \times I_{n_x}. \quad (1)$$

These restrictions are usually motivated by physical plausibility (minimum/ maximum thickness, mass, stiffness, ...). The simulation model

$$\xi: \mathbf{X} \rightarrow \mathbf{Z}: \underline{x} \mapsto \underline{z} \quad (2)$$

maps the input space to the result space \mathbf{Z} . Usually, this space is parametrised as well, thus n_z result parameters (synonyms: output, fitness, response) exist, which leads to a result space $\mathbf{Z} \subset \mathbb{R}^{n_z}$. For applications in mechanical or structural engineering, result parameters are e.g. displacements, stresses and strains. The parametrisation of the result is important, due to the manifold result quantities in time dependent finite element analysis. Therefore, significant (e.g. maximum displacement) or cumulative (e.g. mean displacement) meta parameter are considered. An important characteristic property of the simulation model ξ is that only point-to-point relations are possible. Thus, continuous approaches are not applicable and a sampling-based evaluation needs to be utilized.

1.2 Data mining methods

Data mining methods are used to explore existing data sets and generate knowledge and information about the underlying (but unknown) relationships of input and output data. In the field of application described in this contribution, the data has to be generated. Therefore, methods in context of the Design of Experiments (DoE) are utilized to sample the input space according to Eq. (1) by n_{sim} simulation points. These simulation points are a set \mathcal{X} of input vectors and a set \mathcal{Z} of related result vectors. Due to constraints in the result space, the sample set can be split into permissible and non-permissible samples. This means, the total sample is the union of these two subsets

$$(\mathcal{X}, \mathcal{Z}) = (\mathcal{X}, \mathcal{Z})_{\text{perm}} \cup (\mathcal{X}, \mathcal{Z})_{\text{np perm}}. \quad (3)$$

The applied sampling scheme is responsible for the effectiveness, i.e. ensuring a minimum number of samples in the full input space. The simplest method is to evaluate a simulation model based on high dimensional grids. More effective are space filling designs, aiming uniform distributed samples. Common algorithms for these sampled random numbers are ‘Latin Hypercube sampling’ [McKay, Conover and Beckmann (1979)] and ‘SOBOL’ sequences’ [Sobol’ (1967)].

The methods applied for data mining are outlier analysis [Breunig, Kriegel, Ng et al. (2000)], cluster analysis [Halkidi, Batistakis and Vazirgiannis (2001)] and classification. Furthermore, sensitivities and correlations can be computed for the existing data.

1.3 Machine learning

In engineering applications, the computation of the mechanical model, e.g. by the finite element method, is highly time consuming and for various evaluations (e.g. sensitivity analysis, uncertainty analysis) a large number of model computations is necessary. To

overcome this disadvantage, the research area machine learning or ‘meta-modelling’ provides multiple methods for an approximative model computation [Siddique and Adeli (2013); Simpson, Poplinski, Koch et al. (2001)]. The mechanical model ξ is represented by a meta-model

$$\xi^* : \mathbf{X} \rightarrow \mathbf{Z} : \underline{x} \mapsto \underline{z}^*, \quad (4)$$

such that the original is

$$\xi(\underline{x}) = \xi^*(\underline{x}) + \varepsilon, \quad (5)$$

aiming a minimal error ε between mechanical model and approximation

$$\min \varepsilon = \min | \xi(\underline{x}) - \xi^*(\underline{x}) | \forall \underline{x} \in \mathcal{X}. \quad (6)$$

Commonly, artificial neural networks [Siddique and Adeli (2013)], radial basis function networks [Jin, Chen and Simpson (2001)] or support vector regression [Cherkassky and Ma (2004)] are used. A simpler approach is the polynomial approximation. For these methods, several implementations (e.g. ‘libSVM’ [Chang and Lin (2011)]) exist and can be utilized as surrogate model. Details about the methods applied in this paper (artificial neural networks and polynomial approximations) can be found in Section 4.1.

Remark *The procedure described in this contribution is based on non-adaptive meta-models. This means, the sample set is pre-computed and the meta-model is trained on the basis of this data. Adaptive meta-models integrate the sampling and training in the usage phase [Dubourg (2011)]. Due to the adaptivity, they perform better for highly non-linear problems but are more complicated in implementation and usage.*

1.4 Sampling-based sensitivity measures

Sensitivity analysis is the quantification of the influence of each input parameter to the result parameters [Saltelli, Chan and Scott (2008)]. In general, it is possible to distinguish between global and local sensitivity measures. Locally, the gradient of the simulation model ξ gives information about the influence of each parameter [Sobol’ and Kucherenko (2009)]. For the numerical design, this method is not applicable and the variance-based SOBOL’ index [Sobol’ (2001)] or the frequency-based measure FAST (FOURIER amplitude sensitivity test) [Saltelli, Tarantola and Chan (1999)] can be applied alternatively. The measures are computed on the basis of specific sampling schemes and need a high amount of model evaluations. The variance of the input parameter is predefined on the basis of informative or non-informative random numbers. To quantify the robustness of one selected design, informative random numbers (e.g. normal distribution) can be used. For the design process analysed in this contribution, no information should be considered and, therefore, a non-informative uniform distribution is applied.

2 Introduction of the guiding example

2.1 Clinching process

Clinching is one of the common mechanical joining technologies that can be found in car body production and household appliance (refrigerators, washing machines etc.). It can be classified as a manufacturing process, more detailed as a joining technology or specific as joining by forming, such as hemming or riveting. The main advantage of clinching is that no additional part is necessary (in opposite to riveting) to join the blank sheets. Furthermore, a prepunched hole is not required. It is possible to join blank sheets with different material, for example aluminium and steel. In comparison to welding, no heat is supplied to the joining zone.

For the clinching process, special tools are required: A punch, a die (several types exist, such as round point dies, flat dies or dies with movable blades) and a blank holder. In the first step, the blanks are positioned and clamped between the blank holder and the top of the die. The blank holder prevents a take-off of the blanks and supplies the push out force for removing the punch out of the blanks. In some cases, an additional lower blank holder is use, in order to push the clinch joint out of the die cavity after the clinching process. The upsetting step (see II. in Fig. 1) is characterized by moving the punch downwards until the die-sided sheet metal is in contact with the die. In the last step, the punch is penetrating the material to a predefined position so that an interlock is formed. In order to get a strong clinch joint, the clinch point should have a large neck thickness. A large interlock provides high cross tension strength and prevents unbuttoning under shear load.

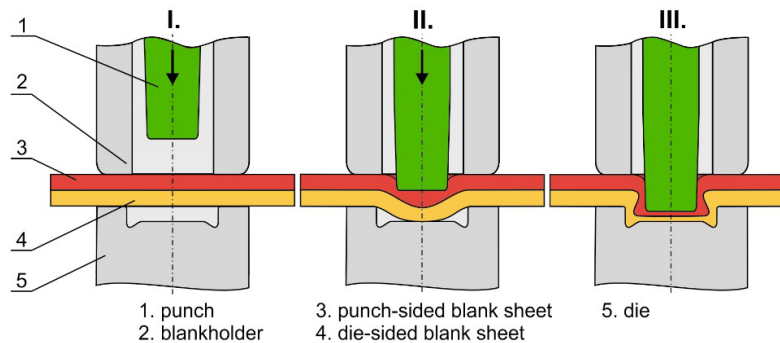


Figure 1: Steps of the clinching process

2.2 Numerical model and description of parametrisation

Simulation In order to save simulation time and getting practical results, the simulation model is a 2D-model with axisymmetric boundary conditions, because of the rotational

symmetry of geometry and loads (see Fig. 2). Nevertheless, it is possible to compute 3D-models, when non-symmetric geometries or loads occur. The used simulation type is Lagrangian incremental with Newton-Raphson iteration and an automatic remeshing. That means, if one rigid part or mesh penetrates another or the used mesh is highly distorted, a remeshing is executed automatically. The material model of the sheets is elasto-plastic, to get springback effects after the joining process. The tools are defined as rigid objects, where the die is fixed and the punch is moving at constant speed. The blank holder is coupled to the punch by pretensioned springs with linear stiffness.

The mechanical properties of the considered material (construction steel S350GD) are determined in tensile tests and transferred to simulation software as pairs of variates for true strain and yield stress (yield surface). The friction between the sheet metal and tools – but also the sheets itself - is very complex. In the simulation, the friction conditions are defined as a constant shear factor during the whole process, which is state of the art in metal forming simulation. Further information can be found in Landgrebe et al. [Landgrebe, Kropp, Gehrke et al. (2017); Landgrebe, Mauermann and Kropp (2017)].

Validation To make sure that the simulation results match with experimental data, three configurations with different sheet thickness ratios where joint ($t_1 + t_2 \in \{3 + 2 \text{ mm}; 2.5 + 2.5 \text{ mm}; 2 + 3 \text{ mm}\}$). This comparison is done by considering the contour geometry of the cross-section and the load-stroke-data of the joining process. The very good agreement between simulation and experiment can be seen in Figs. 2 and 3.

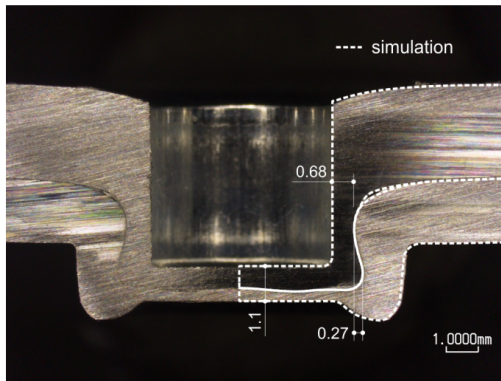


Figure 2: Clinching construction steel S350GD ($t_1 = 3 \text{ mm}$, $t_2 = 2 \text{ mm}$)

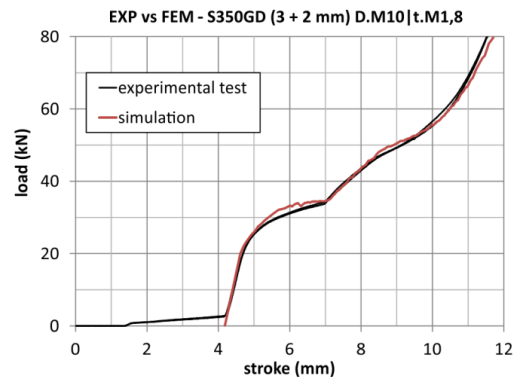


Figure 3: Comparison between simulation results and experimental data

Geometric tool parameters and output parameters In the present paper, the focus is on the interaction of geometric tool parameters (see Fig. 4).

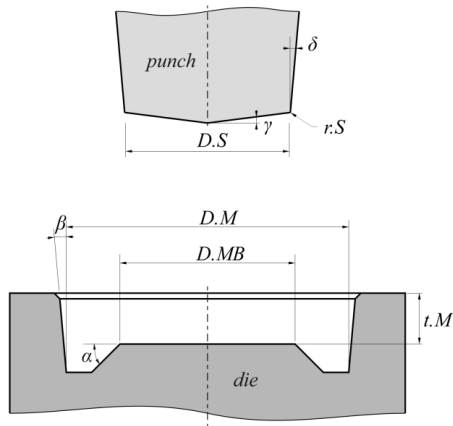


Figure 4: Geometric input parameters of clinch tools

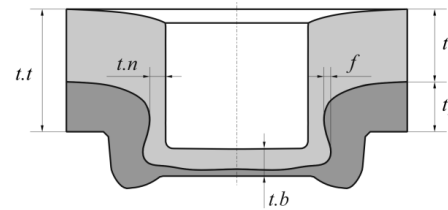


Figure 5: Geometric parameters of a clinched joint

In Tab. 1, the investigated parameters for the die and the punch geometry are shown. Investigated is a fixed total sheet thickness of $t.t = 5$ mm, with variable ratio of the single sheet thickness x_{t1} . To avoid samples without reference to reality, some parameters are given in a relative manner. For example, it is not practicable using a punch diameter $D.S$ that is larger than the diameter of the die $D.M$. Such that, the punch diameter is related to the die diameter $D.S = x_{D.S_rel} \cdot x_{D.M}$.

The response variables interlock z_f and neck thickness $z_{t.n}$ (see Fig. 5) are significant for the quality of a clinching joint. The overall objective is to find geometries with maximal interlock and neck thickness constrained by specific thresholds.

3 Exploration of data

The given initial design space $(\mathcal{X}, \mathcal{Z})_{init}$ following from the data in Tab. 1 is the basis for a DoE. Therefore, 9101 samples of the numerical simulation of the clinching process are carried out on the basis of Latin Hypercube Sampling (LHS). The sample set was reduced by removing non-physical samples. It is the main goal of the numerical simulations to derive general properties of the physical process with respect to preferred geometric properties, described by two result quantities. The evaluation of the result values leads to the conclusion that not every design vector x is permissible regarding the desired properties. The existing data set is investigated with data exploration techniques, in order to enhance the general understanding of the physical process as well as validate upcoming results of the surrogate models by comparison to characteristic quantities based on the actual data set.

Table 1: Input and response parameters of the simulation model

#	variable	description	min. value	max. value
input parameters				
1	$x_{D.M}$	die diameter	7.5 mm	12.5 mm
2	$x_{t.M_rel}$	die depth in relation to total sheet thickness	0.2	0.6
		$x_{t.M_rel} = \frac{t.M}{t_1+t_2}$		
3	$x_{D.MB_rel}$	die diameter bottom in relation to punch diameter	0.8	1.2
		$x_{D.MB_rel} = \frac{D.MB}{D.S}$		
4	$x_{alpha.M}$	angle die bottom	15°	45°
5	$x_{beta.M}$	angle die side face	0°	5°
6	$x_{D.S_rel}$	punch diameter in relation to die diameter	0.5	0.75
		$x_{D.S_rel} = \frac{D.S}{x_{D.M}}$		
7	$x_{R.S}$	radius punch	0.25 mm	0.5 mm
8	$x_{gamma.S}$	angle punch face	0°	2°
9	$x_{delta.S}$	angle punch side face	0°	4°
10	x_{t1_rel}	thickness upper sheet in relation to total sheet thickness	0.2	0.8
		$x_{t1_rel} = \frac{t_1}{t_1+t_2}$		
11	$x_{t.b}$	bottom thickness	0.589 mm	5.035 mm
output parameters				
1	z_f	interlock		
2	$z_{t.n}$	neck thickness		

3.1 Permissible design space

Initially, the data set is split into permissible and non-permissible data according to Eq. (3), whereas the constraint is defined by

$$z_f > 0, \quad (7)$$

forcing the existence of an interlock. With respect to Eq. (7), $n_{perm} = 2365$ permissible data points in $(\mathcal{X}, \mathcal{Z})_{perm}$ and, consequently, $n_{nperm} = 6736$ non-permissible in $(\mathcal{X}, \mathcal{Z})_{nperm}$ are obtained.

To have a brief overview of the interdependencies between two parameters, a scatter plot of the data as depicted in Fig. 6 can be used. The upper triangular matrix is related to \mathcal{X}_{perm} , the lower to \mathcal{X}_{nperm} .

With the focus on the permissible data, there are two noticeable issues. First of all, the correlation or more general dependency between the following pairs of parameters is

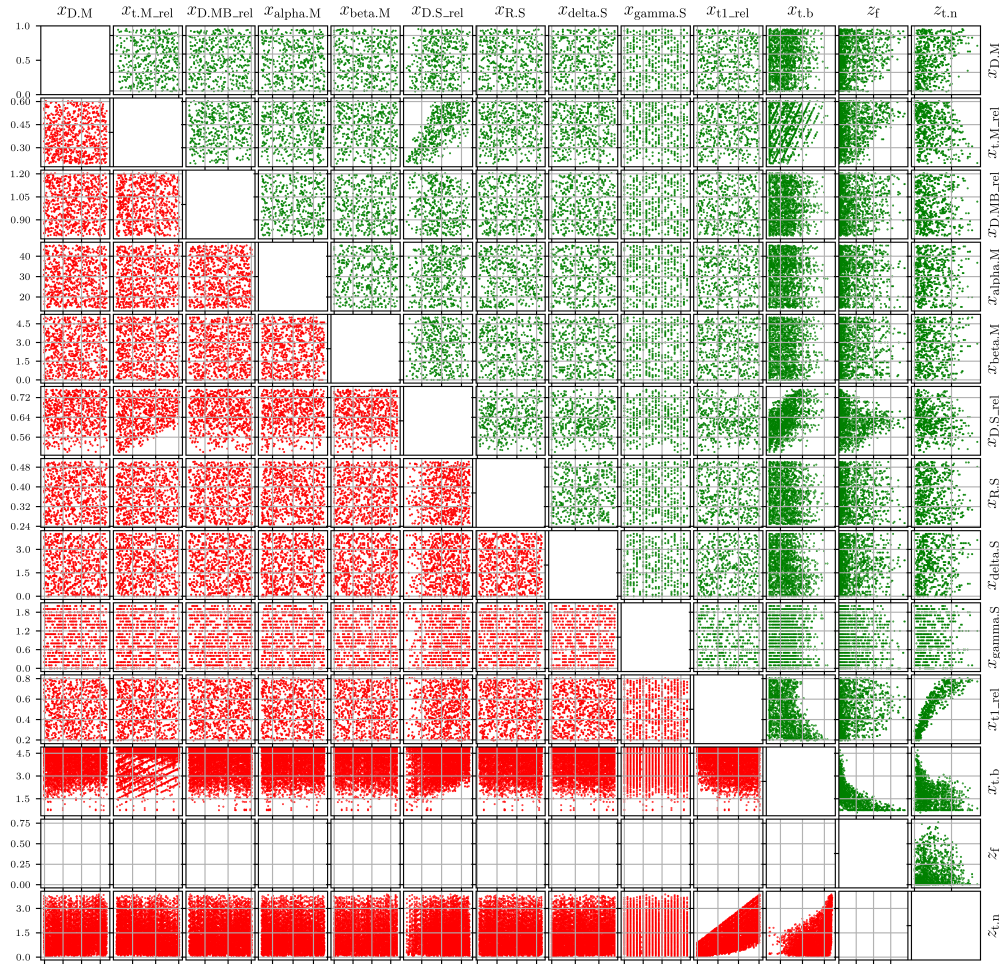


Figure 6: Scatter plot for permissible (green) and non-permissible (red) data

observable

$$x_{D,S,rel} \sim x_{t,M,rel}, x_{t,b} \sim x_{D,S,rel} \text{ and } x_{t,b} \sim x_{t1,rel}. \quad (8)$$

Secondly, the non-permissible data is approximately as equally distributed in \mathbf{X} as the permissible data, except of the correlated parameters. Hence, if an input space \mathbf{X}_{perm} is defined by $\mathbf{X}_{\text{perm}} = [x_{\min,\text{perm},1}, x_{\max,\text{perm},1}] \times \dots \times [x_{\min,\text{perm},11}, x_{\max,\text{perm},11}]$, the permissible design range for each input parameter is equal to the initial ranges in Tab. 1. It is not ensured that $\underline{x} \in \mathbf{X}_{\text{perm}}$ is permissible. Particular with regard to the approximation by a surrogate model, it is expedient to integrate e.g. a classification method. An alternative approach is the computation of design spaces based on permissible points only [Graf, Götz and Kaliske (2018)]. Other names for this method are solution space [Zimmermann and von Hoessle (2013)] or feasible design area [Duddeck and Wehrle (2015)]. If these subsets are

independent intervals for each input variable, a permissible hypercuboid can be computed. A method to compute such a hypercuboid is given in Goetz et al. [Götz, Liebscher and Graf (2012); Graf, Götz and Kaliske (2018)].

For the analysed data set, the permissible hypercuboid is given in Fig. 7 and Eq. (9). The difference compared to the initial design space are emphasized

$$\begin{aligned} \underline{x}_{\min, \text{perm}, \text{HC}} &= [7.453, 0.196, 0.796, 14.7, \mathbf{1.0}, \mathbf{0.55}, 0.248, 0.0, 0.0, 0.195, 0.59], \\ \underline{x}_{\max, \text{perm}, \text{HC}} &= [12.53, 0.604, 1.204, 45.3, 5.0, 0.75, 0.502, 4.0, \mathbf{1.6}, 0.81, \mathbf{1.478}]. \end{aligned} \quad (9)$$

The permissibility is defined according to Eq. (7), whereas the objective is a permissible hypercuboid with maximum number of points inside. The visualisation applied in Fig. 7 is called parallel coordinate plot [Inselberg (1985)]. Hereby each parameter is represented by a separated axis. A parameter vector inside the permissible hypercuboid is represented as line inside the grey marked area. The shown hypercuboid contains 25.6 % of the permissible points, which is a reasonable result.

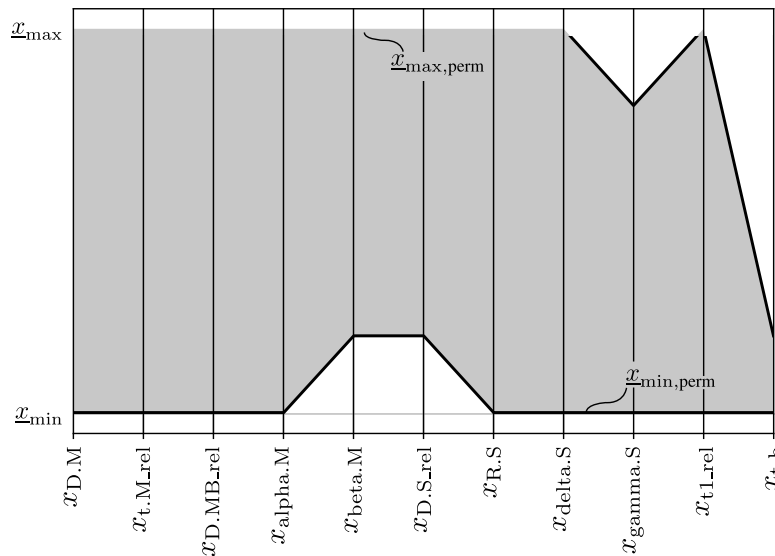


Figure 7: Permissible design space visualised as parallel coordinate plot

The benefit of the computed permissible design space is, that within the design process, the engineer can select any parameter combination inside the permissible design space. A disadvantage is that the usable hypervolume, representing the range of possible designs, is only 10.2% of the initial design space, see Tab. 1.

3.2 Sensitivity analysis

For engineering related design guidelines, the amount of 11 independent parameters is challenging regarding the specification of a suitable design. A sensitivity analysis is carried out in order to identify parameters with major influence on the result quantities. Correlations are evaluated with the goal to substitute one parameter by another for the purpose of parameter reduction. One correlation coefficient as well as two sensitivity coefficients will be briefly introduced and applied to the permissible data set $(\underline{x}, \underline{z})_{\text{perm}}$.

Spearman correlation coefficient The SPEARMAN rank correlation coefficient is commonly applied to assess the relationship between two parameters described by monotonic function and is therefore a non-linear correlation coefficient [Saltelli, Chan and Scott (2008)]. It is defined as

$$r_{\text{SPEARMAN}}(\underline{x}, \underline{z}) = \frac{\sum_{l=1}^{n_{\text{sim}}} (\text{rg}(x_l) - \bar{\text{rg}}_x) \cdot (\text{rg}(z_l) - \bar{\text{rg}}_z)}{\sqrt{\sum_{l=1}^{n_{\text{sim}}} (\text{rg}(x_l) - \bar{\text{rg}}_x)^2 \cdot \sum_{l=1}^{n_{\text{sim}}} (\text{rg}(z_l) - \bar{\text{rg}}_z)^2}}, \quad (10)$$

with the rank $\text{rg}(\square)$ and the mean of the rank $\bar{\text{rg}}_x = \bar{\text{rg}}_z = (n+1)/2$. A coefficient value $|r_{\text{SPEARMAN}}| = 1$ is related to an ideally positive or negative monotonic (non-linear) relation between \underline{x} and \underline{z} . The resulting correlation coefficients r_{SPEARMAN} is depicted in Fig. 8 for each parameter combination where the result parameters are separated by the dashed line.

The correlation assumption by the visual interpretation of Fig. 6 is reassured by following correlation coefficients

$$\begin{aligned} r_{\text{SPEARMAN}}(x_{\text{t.m.rel}}, x_{\text{D.S.rel}}) &= +0.674, & r_{\text{SPEARMAN}}(x_{\text{t1.rel}}, z_{\text{f}}) &= +0.308, \\ r_{\text{SPEARMAN}}(x_{\text{D.S.rel}}, x_{\text{t.b}}) &= +0.548, & r_{\text{SPEARMAN}}(x_{\text{t1.rel}}, z_{\text{t.n}}) &= +0.939, \\ r_{\text{SPEARMAN}}(x_{\text{t1.rel}}, x_{\text{t.b}}) &= -0.328, & r_{\text{SPEARMAN}}(x_{\text{t.b}}, z_{\text{f}}) &= -0.767. \end{aligned} \quad (11)$$

For the further analysis and utilization of the data set, the correlations between input and output parameters are from higher importance. Under the assumption that $|r_{\text{SPEARMAN}}(\underline{x}, \underline{z})|$ can be additionally interpreted as sensitivity measure, $x_{\text{t1.rel}}$ has the major effect to $z_{\text{t.n}}$ and $x_{\text{t.b}}$ to z_{f} . Especially the identified correlation information between the input parameters $x_{\text{t.m.rel}} \sim x_{\text{D.S.rel}}$ and, consequently, the reduced permissible design space (see Fig. 6) is decisive for the training, evaluation and utilization of surrogate models.

Correlation relation estimation Additional to the correlation analysis, an estimation of the sensitivities is utilized by the application of a correlation relation estimation.

According to Siebertz et al. [Siebertz, van Bebbber and Hochkirchen (2010)], the correlation relation can be defined as

$$\text{KV}_i = \frac{\text{Var}[E[Z|X_i]]}{\text{Var}[Z]}, \quad 0 \leq \text{KV}_i \leq 1, \quad (12)$$

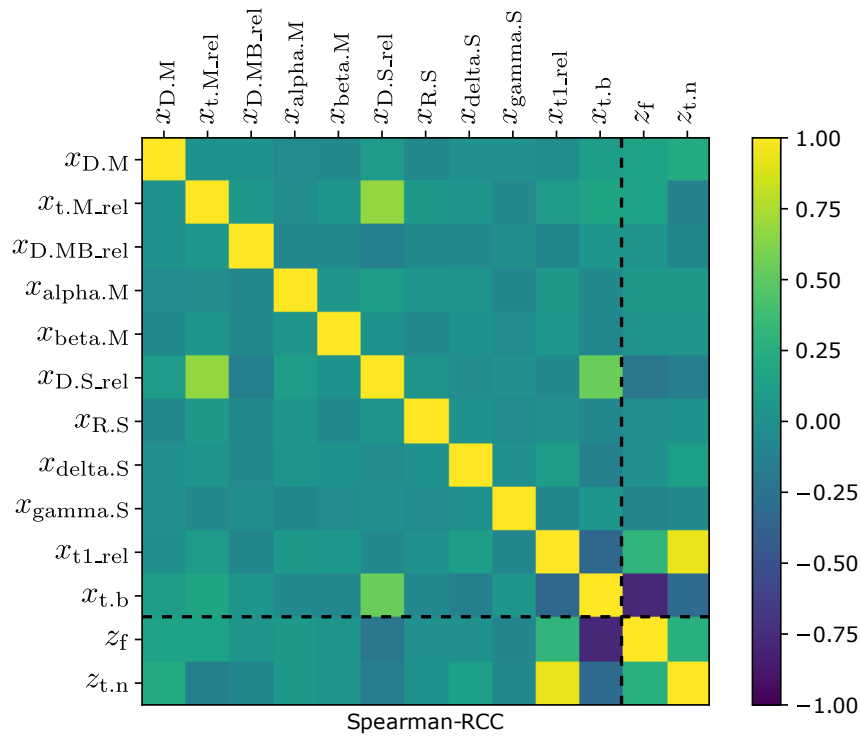


Figure 8: Correlation matrix (SPEARMAN rank correlation coefficient) for input and output parameters

analogous to the variance-based sensitivities measures. A sampling-based estimator for the sensitivity measure is proposed in Siebertz et al. [Siebertz, van Bebber and Hochkirchen (2010)]. This method itself is not applicable to existing data, but the general concept has been adapted to a variance-based sensitivity measure for existing data KWest (KWestimation).

Each input parameter is separated into p intervals $I_{i,k}, k \in \{1, \dots, p\}$ with the associated data set

$$(\underline{\mathcal{X}}, \underline{\mathcal{Z}}_j)_{i,k} = \bigcup_{l=1}^{n_{\text{perm}}} (x_l, z_{j,l}) \mid x_l \in \mathbf{X}_{i,k} \tag{13}$$

for each output parameter z_j . Hence, the conditional mean values

$$\overline{\underline{\mathcal{Z}}}_{i,j,k} = \frac{1}{\#\{\underline{\mathcal{Z}}_{i,j,k}\}} \cdot \sum \underline{\mathcal{Z}}_{i,j,k} \tag{14}$$

are utilized to approximate the correlation relation with the variance of the mean values by

$$S_{x_i|z_j}^{KVest} = KVest_{i,j} = \frac{\hat{s}(\overline{\mathcal{Z}_{i,j,k}})^2}{\hat{s}(\overline{\mathcal{Z}_j})^2} \approx \frac{\text{Var}[E[Z_j|X_i]]}{\text{Var}[Z_j]}. \tag{15}$$

The presented sensitivity measure is interpretable as first order SOBOL’ indices, see Section 5.1. Assuming a large number of data samples as well as sub spaces, it holds $S_{x_i|z_j}^{KVest} \approx S_{x_i|z_j}^{SOBOL}$, whereas a small data set is still applicable to quantify the significance of input parameters even for non-linear dependencies.

For each output parameter, the computed sensitivities for the most sensitive input parameters are shown in Tab. 2. Especially the variance of $z_{t,n}$ seems to be solely depending on x_{t1_rel} and weakly $x_{t,b}$. According to the KVest measures, the other remaining input parameters are insignificant to the output parameter. Compared to the correlation evaluation with the SPEARMAN coefficient (see Eq. (11)), the same two main contributors are identified.

Table 2: Three major influences in descending order

interlock z_f			neck thickness $z_{t,n}$		
parameter	$S_{x_i z_f}^{KVest}$	$S_{x_i z_f}^{EASI}$	parameter	$S_{x_i z_{t,n}}^{KVest}$	$S_{x_i z_{t,n}}^{EASI}$
$x_{t,b}$	0.44	0.59	x_{t1_rel}	0.61	0.68
$x_{D.S_rel}$	0.15	0.11	$x_{t,b}$	0.16	0.08
x_{t1_rel}	0.11	0.10	$x_{D.M}$	0.07	0.08
$1 - \sum_{i=1}^{n_x} S_{x_i z_f}^{\square}$	0.30	0.20	$1 - \sum_{i=1}^{n_x} S_{x_i z_{t,n}}^{\square}$	0.16	0.16

EASI For the purpose of comparison and validation of the identified correlation and sensitivity values, another and methodical different approach is used as sensitivity measure. Originally, the ‘effective algorithm for computing global sensitivity indices’ (EASI) has been introduced by [Plischke (2010)] as a sensitivity measure for existing data of non-linear systems. The method is adapted to the general concept of FAST, which is analysing the input space by frequency dependent characteristic functions and the map

$$G_{\omega}(s) = \frac{1}{\pi} \arccos(\cos(2\pi \cdot \omega \cdot s)). \tag{16}$$

Due to permutation and resorting of existing data $(\mathcal{X}, \mathcal{Z})$, the EASI approach leads to the approximation of Eq. (16) for the frequency $\omega = 1$. At the beginning, one input parameter x_i and one output parameter z_j are increasingly sorted to obtain an ordered vector

$(x_{i,l}, z_{j,l})' = (x_i, z_j)_l \mid x_{i,l} \leq x_{i,l+1} \forall l = 1, 2, \dots, n_{\text{perm}}$. In order to approximate a triangular shaped function, all odd indices of $(x_i, z_j)_l'$ in increasing order are followed by all even indices in decreasing order, such as

$$(x_{i,l}, z_{j,l})'' = \begin{cases} (x_i, z_j)_{2l-1}' & l \leq \frac{n+1}{2} \\ (x_i, z_j)_{2(n_{\text{sim}}+1-l)}' & l > \frac{n+1}{2} \end{cases} \quad l = 1, 2, \dots, n_{\text{perm}}. \quad (17)$$

This specific shuffling leads to a triangular-shape vector, which is in analogy to the FAST sampling at $\omega = 1$. Since the permutation of the output parameter is conjoined to the input permutation, the resonances of period $\omega = 1$ and its higher harmonics in the power spectrum are used to determine the sensitivity. Based on the complex coefficients

$$c_m = \sum_{l=1}^{n_{\text{sim}}} z_{j,l}'' \cdot \exp \left[-\frac{2\pi \cdot i}{n_{\text{sim}}} \right]^{(l-1) \cdot m}, \quad i^2 = -1, \quad (18)$$

of the discrete Fourier transformation, the first order sensitivity index is computed by

$$S_{x_i|z_j}^{\text{EASI}} = \frac{\sum_{m=1}^M |c_m|^2}{\sum_{m=1}^{n_{\text{sim}}/2} |c_m|^2}. \quad (19)$$

According to Plischke [Plischke (2010)], the number of higher harmonics is set to $M = 6$. The computed sensitivities are given in Tab. 2.

Both introduced sensitivity measures only provide an approximation for first order sensitivity. The sum of higher order sensitivities (total sensitivity) can be estimated by $1 - \sum_{i=1}^n \sum_{j=1}^n S_{x_i|z_j}^{\text{EASI, KVest}}$. As can be seen in Tab. 2, the amount of higher order sensitivities is significant and cannot be neglected. For both result values, the determined sensitivities are depicted in Fig. 9. Evidently, the qualitative results of both measures are similar to each other or equal regarding the descending order of the sensitive input parameters.

Self-organizing map An entirely different approach in correlation analysis is the evaluation of Self-organizing maps (SOM). Introduced by KOHONEN, SOM try to adapt the biological brains ability to map complex high-dimensional data to a low-dimensional (2D) representation of information, thus SOM: $\mathbb{R}^{n_x} \rightarrow \mathbb{R}^2$. Topological properties of the data are hereby preserved, which allows the identification of e.g. clusters or correlation behaviour. Possible evaluation methods for cluster identification or spatial distribution of data are described in Liebscher et al. [Liebscher, Witowski and Goel (2009); Ultsch (2003)]. In this contribution, component maps, based on an orthogonal neural grid of 30×30 neurons, are utilized and the resulting component charts are separately depicted in Fig. 10. Based on the grid representation of the neural network, the parameter value of a neuron

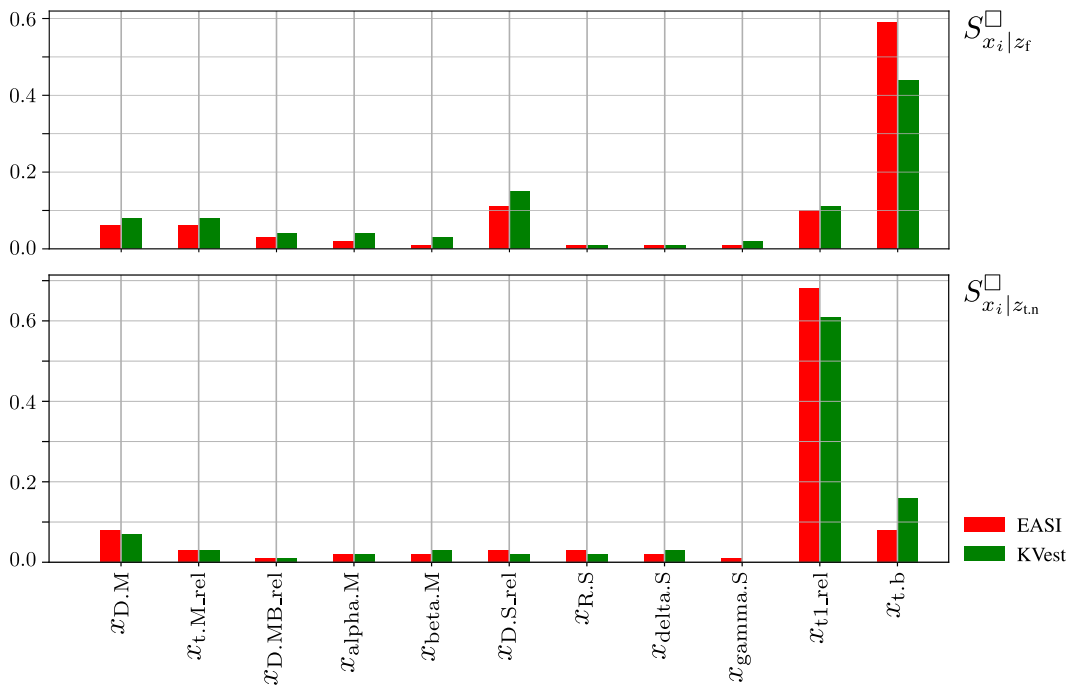


Figure 9: Result of sensitivity analysis with Kvest and EASI for z_f (interlock) and $z_{t,n}$ (neck thickness)

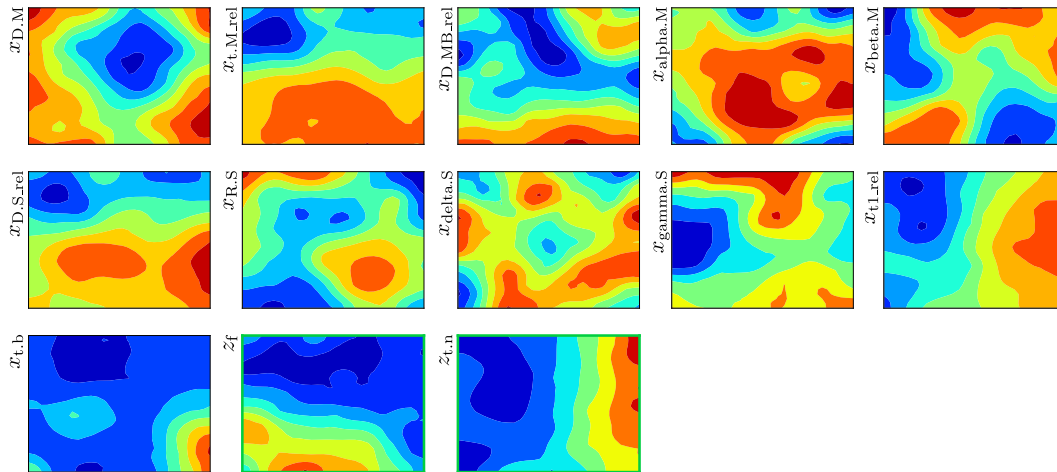


Figure 10: Component map of Self-Organizing map trained for permissible data $(\underline{\mathcal{X}}, \underline{\mathcal{L}})_{perm}$ (response parameters are highlighted in green)

are represented at the neurons position in the grid. Under the assumption of a considerably good fit of the network, correlation analysis can be provided, since at each map position the actual data space is represented as well.

No correlation is visualized by two orthogonal component charts, whereas either positive or negative correlation is represented by equal or inverse gradients of the components. Those observations can be done globally over the map and, therefore, the entire data space, or locally for a partial area of the SOM.

Regarding the data set, multiple interdependencies can be identified. The response values seem to be independent to each other, since charts are clearly orthogonal to each other, whereas the positive correlation between $z_{t,n}$ and x_{t1_rel} can be derived from the equally oriented trend lines. Same applies for the dependency between x_{D,S_rel} and x_{t,M_rel} . The distinctive negative correlation between $x_{t,b}$ and z_f is not clearly visible, but can be confirmed by SOM. Due to the component charts, see [Malone, McGarry, Wermter et al. (2005); Mostafa (2009)], low (blue) parameter values of $x_{t,b}$ comply with the total range of z_f , but increasing parameter values lead to a decrease of the output parameters (see lower left and right corner).

Summary of data mining From the previously discussed results, the following conclusions can be drawn:

- independent measures (KVest and EASI) yield the same results,
- most significant parameter for result interlock z_f : $x_{t,b}$ (bottom thickness), x_{D,S_rel} (punch diameter in relation to die diameter) and x_{t1_rel} (thickness upper sheet in relation to total sheet thickness),
- most significant parameter for result neck thickness $z_{t,n}$: x_{t1_rel} (thickness upper sheet in relation to total sheet thickness), $x_{t,b}$ (bottom thickness) and $x_{D,M}$ (die diameter),
- high amount of parameter interaction is expected,
- permissible design space cannot be identified on the basis of the scatter plot,
- dependencies (correlations) in the permissible and non-permissible data set are identifiable.

4 Meta-modelling

In the following, two different machine learning methods (artificial neural network and response surface) are discussed and applied to the presented example. Furthermore, the meta-models are evaluated and visualised.

4.1 Artificial neural networks and polynomial approximation

Artificial neural networks An artificial neural feed-forward network with one hidden layer (with n_v neurons, see Fig. 11) can be written as weighted sum of the output of the neurons

$$\xi^*(x) = \sum_{v=1}^{n_v} \underline{\beta}_v \cdot G(\underline{w}_v, \underline{\theta}_v, x). \tag{20}$$

The vector $\underline{\beta}$ contains the weighting factors between hidden layer and output neuron. The function G is the processing of one neuron, see Fig. 12. It is $G(\underline{w}, \underline{\theta}, x) = \varphi(\xi, \theta) = \varphi(\xi(\underline{w}, x), \theta)$. The neuron consists of two separated functions. A common propagation function is the weighted sum of all input signals $\xi(\underline{w}, x) = \sum_{i=1}^{n_x} w_{v,i} \cdot x_i$. The weights \underline{w} representing the strength of influence for each input neuron to each hidden neuron separately. The activation function φ can be formulated by various functions, e.g. hyperbolic tangent or binary threshold. In this study, an unipolar function

$$\varphi_{uni,\theta}(\xi, \theta) = \frac{1}{1 + e^{-(\xi + \theta)}} \tag{21}$$

is used. This function depends on the output of the propagation function ξ and a bias value θ .

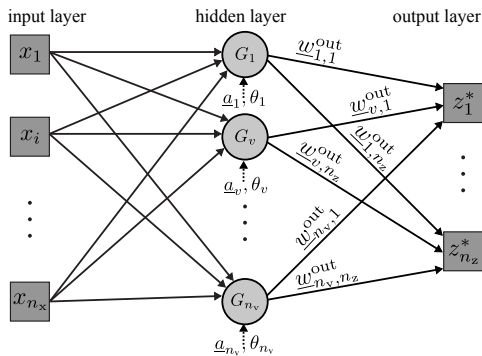


Figure 11: Generalised neural network with one hidden layer

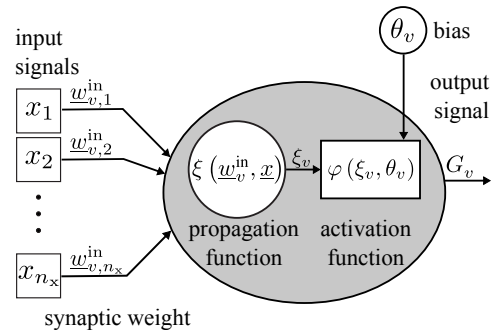


Figure 12: Construct of hidden neuron i

The training or learning of the ANN is the definition of appropriate weighting factors for a preliminary defined network architecture (i.e. number of neurons, number of layers, activation function) see Hagan et al. [Hagan and Menhaj (1994); Siddique and Adeli (2013); Wilson and Martinez (2003)].

Polynomial approximation The polynomial approximation is mostly called ‘Response Surface Method (RSM)’. The main idea is to represent the data by a polynomial of degree n .

Usually, the degree is $n = 1$ for linear approximation or $n = 2$ for quadratic approximation

$$\xi^*(\underline{x}) = \beta_0 + \sum_{i=1}^{n_x} \beta_i x_i + \sum_{i=1}^{n_x-1} \sum_{j=i+1}^{n_x} \beta_{ij} x_i x_j + \sum_{i=1}^{n_x} \beta_{ii} x_i^2. \quad (22)$$

The coefficient β_0 is the constant, $\beta_{i,j,ii}$ are the coefficients for the linear, mixed and quadratic terms, respectively.

The training procedure is the computation of vector $\underline{\beta}$ on the basis of minimization of the root mean square error by an HESSIAN matrix, see Myers et al. [Myers, Montgomery and Anderson-Cook (2009)]. Thereby, the most common assumption for the error ε in Eq. (5) is zero mean, yielding the ordinary least-squared estimator of $\underline{\beta}$.

4.2 Selection and training of meta-models

Meta-models contain various parameters, which need to be found during a training process. Due to different characteristics (e.g. size, dimensionality, complexity, white noise, ...), data sets cannot be considered by one general meta-model. Thus, it is challenging for meta-modelling to select a type of model, the architecture of the model and the training parameters of the model. A common method is to analyse the performance of different meta-models for the same data set. To have possibility for validation, the data set is split into a set used for training and another for testing. The approximation error depends on the selection of training and test data. To overcome this, the k -fold cross-validation (CV) [Arlot and Celisse (2010); Geisser (1975)] is commonly used. Thereby, the data set is split into k subsets

$$(\underline{\mathcal{X}}, \underline{\mathcal{Y}}) = (\underline{\mathcal{X}}, \underline{\mathcal{Y}})_1 \cup (\underline{\mathcal{X}}, \underline{\mathcal{Y}})_2 \cup \dots \cup (\underline{\mathcal{X}}, \underline{\mathcal{Y}})_k \quad (23)$$

and the training is repeated k times. Typically, the number of subsets is selected within $k \in \{5, 10\}$.

The comparison of different meta-models is based on a mean error

$$\bar{\varepsilon}_{\text{RMS}} = \frac{1}{k} \sum_{i=1}^k \varepsilon_{i,\text{RMS}}. \quad (24)$$

The error measure ε_{RMS} is given in Eq. (26). The k -fold CV is basis for an automatic selection process.

For the solution analysed in this contribution, the meta-modelling is performed for both result quantities z_f and $z_{t,n}$ independently. The training is done for a polynomial approximation (linear and quadratic) according to Eq. (22), support vector regression using

'libSVM' [Chang and Lin (2011)] and ANN according to Eq. (20). The finding of an optimal ANN architecture is included in the automatic select process. These neuron-layer combinations are based on the number of neurons in a first hidden layer of $\{1 - 25\}$ and for a second hidden layer of $\{0 - 25\}$. By holding the condition that the number of hidden neurons in the second hidden layer is smaller/equal that in the first hidden layer, 219 different architectures are observed.

The training, i.e. the optimisation of neuron bias values and connecting weights, can be done by back-propagation algorithms. These algorithms are very slow, which is critical due to the high amount of observed models. Therefore, the LEVENBERG-MARQUARDT-algorithm can be used [Hagan and Menhaj (1994); Levenberg (1944); Marquardt (1963)]. This algorithm is very fast but tends to over-learning. This disadvantage is due to the repeated training in the framework of k -fold CV not relevant.

The analysis is performed on an 'Intel i7-4790' CPU within 40 hours for each result quantity. As result of the observed meta-models, ANNs perform best. The best architectures (number of input neurons – hidden layer neurons – hidden layer neurons – output neurons) are for z_f : (11 – 25 – 16 – 1) and for $z_{t,n}$: (11 – 22 – 18 – 1).

4.3 Quality evaluation and visualisation

The quality of meta-models is evaluated by characteristic measures. The error to be observed is the difference between original result and the approximation. The error for a simulation point l is

$$\varepsilon_l = |z_l - \underline{z}_l^*|. \quad (25)$$

The following two measures are mainly used. The root mean square error (RMS) is

$$\varepsilon_{\text{RMS}} = \sqrt{\frac{1}{n_{\text{sim}}} \cdot \sum_{l=1}^{n_{\text{sim}}} (\varepsilon_l)^2} \quad (26)$$

A disadvantage is, that the value of the RMS depends on the order of magnitude for the observed result. This means, only a relative evaluation of the approximation quality is possible. But different meta-models for the same data set can be evaluated relatively to each other. Another important measure is the coefficient of determination R^2 (also called CoD [Most and Will (2010)])

$$\varepsilon_{R^2} = \frac{\sum_{l=1}^{n_{\text{sim}}} (\underline{\mathcal{L}}_l^* - \underline{\mathcal{L}})^2}{\sum_{l=1}^{n_{\text{sim}}} (\underline{\mathcal{L}}_l - \underline{\mathcal{L}})^2} = 1 - \frac{\sum_{l=1}^{n_{\text{sim}}} (\underline{\mathcal{L}}_l^* - \underline{\mathcal{L}}_l)^2}{\sum_{l=1}^{n_{\text{sim}}} (\underline{\mathcal{L}}_l - \underline{\mathcal{L}})^2} = \frac{\text{explained sum of squares}}{\text{total sum of squares}}. \quad (27)$$

For the analysed data set, the quality measures are given in Tab. 3. Additionally to the ANNs, a polynomial meta-model with quadratic polynomial degree is given. The polynomial approximation follows the formulation in Eq. (22) in general. However, only the most significant input parameters (based on correlation measures) are considered in the utilized polynomial approximation.

Table 3: Comparison of the approximation quality for ANN and polynomial

	interlock z_f		neck thickness $z_{t,n}$	
error measure	ANN	polynomial	ANN	polynomial
ε_{RMS}	0.0084	0.0472	0.0039	0.0386
ε_{R^2}	0.9977	0.9204	0.9992	0.9868

The error measures in the table show the disadvantage of the measure ε_{R^2} . For the polynomial approximation, a value of $z_f = 0.92$ indicates a reasonable approximation, but Fig. 13(b) shows that the approximation quality is not reasonable. The measure ε_{RMS} indicates the very good approximation quality of the ANNs, which can be validated by Fig. 13(a) and Fig. 13(c). The graphs in Fig. 13 show the predicted results z_i^* and the original results z_i for all sample data.

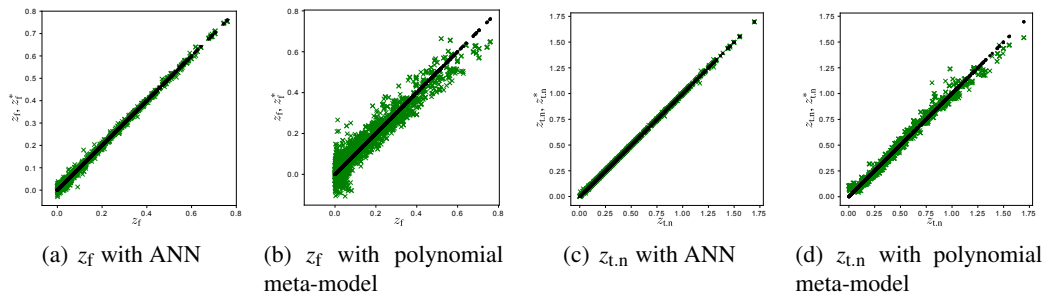
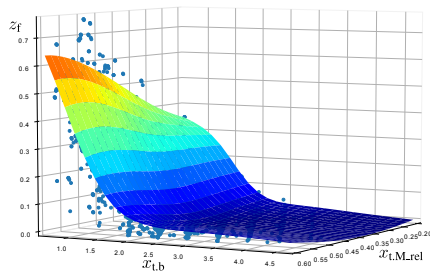


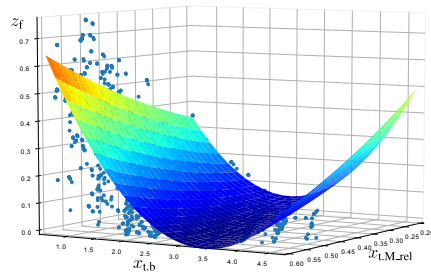
Figure 13: Quality assessment of analysed meta-models (black: z_i , green: z_i^*)

It is common to use 3D visualisations depict the meta-model, which is challenging for the multi-dimensional input space (here 11-dimensional). The others (not shown dimensions) need to have fixed values, such that $\frac{n_x^2 - n_x}{2}$ possibilities for visualisations exist. Thus, any visualisation of multi-dimensional data in 3D is limited. In Figs. 14 and 15, two input parameter are selected, separated for each result. Additional to the meta-model result (continuous plot), the original data set is shown.

Most of the scatter of the input data can be explained by the two selected input parameters. In contrast, Fig. 16 has two selected input parameters where the meta-model cannot explain the scatter. These parameters can be interpreted as locally (due to the fixed other parameters) non-sensitive.

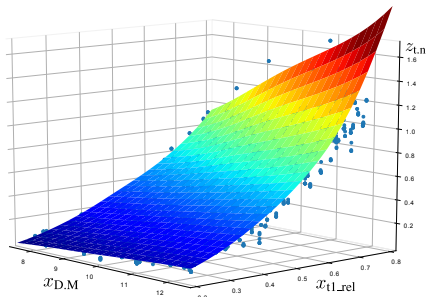


(a) ANN

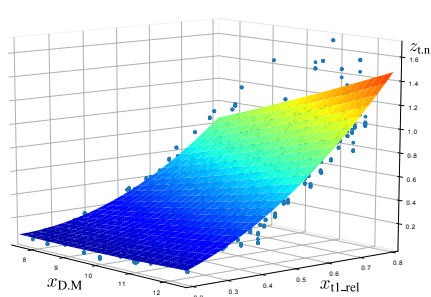


(b) Polynomial

Figure 14: 3D-visualisation for z_f , $\underline{x} = [10.0, [0.2, 0.6], 1.0, 30.0, 2.5, 0.63, 0.38, 2.0, 2.0, 0.5, [0.6, 4.7]]$ and sample set (blue points)



(a) ANN



(b) Polynomial

Figure 15: 3D-visualisation for $z_{t,n}$, $\underline{x} = [[7.45, 12.53], 0.4, 1.0, 30.0, 2.5, 0.63, 0.38, 2.0, 2.0, [0.20, 0.81], 2.64]$ and sample set (blue points)

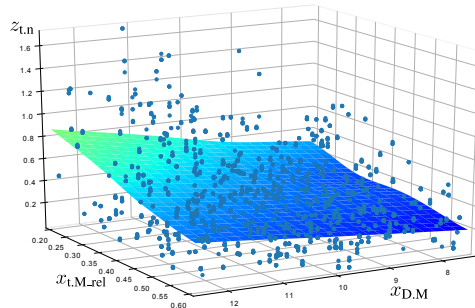


Figure 16: Non-useful 3D-visualisation for $z_{t,n}$, $\underline{x} = [[7.45, 12.53], [0.2, 0.6], 1.0, 30.0, 2.5, 0.63, 0.38, 2.0, 2.0, 0.5, 2.64]$ and sample set (blue points)

5 Sensitivities

In this section, the most common sensitivity measures are described, computed and discussed for the clinching process. Namely, these measures are the SOBOL' indices of first order $S^{\text{SOBOL}'}$ and the total SOBOL' indices $S^{\text{SOBOL}',T}$. The sensitivities are computed using the developed meta-models. The results are compared to the measure for existing data S^{KVEST} (see Section 3.2) and the measure S^{COP} . The Coefficient of Prognosis (CoP) is used in [OptiSLang (2011)] and computed for the polynomial meta-model. Furthermore, the functional behaviour of the total SOBOL' index called sectional sensitivity measure shows the change of influence for each input parameter.

5.1 Sensitivity measures

For variance-based sensitivity measures, it can be distinguished between effects of first and higher order. Effects of first order $S_{x_i|z_j}^{\square}$, also called main effects, quantifying the influence of one parameter x_i to the variance of the result z_j . Effects of higher order $S_{x_i,\dots,p|z_j}^{\square}$ capturing the influence of two or more input parameters x_i,\dots,p to variance of the result z_j . The overall influence of one input parameter is called total sensitivity. The computation of the SOBOL indices, i.e. the solution of high dimensional integrals, can be done by Monte-Carlo simulation or more efficient on the basis of polynomial chaos expansion [Sudret (2008)].

SOBOL' index The SOBOL' index of first order [Sobol' (2001)] is defined as

$$S_{x_i|z_j}^{\text{SOBOL}'} = \frac{\text{Var}_{x_i}[\mathbb{E}[z_j|x_i]]}{\text{Var}[z_j]}, \quad (28)$$

with the result quantity z_j and the input quantity x_i . The expected value of z_j under the condition of occurrence for a specific x_i is $\mathbb{E}[z_j|x_i]$. The variance overall possible x_i is Var_{x_i} .

The variance of the result $\text{Var}[z_j]$ is designated as total variance. This measure is also called measure of importance.

Total SOBOL' index The cumulative influence of all lower level sensitivities (i.e. first order, second order, ...) can be computed by the total SOBOL' index [Homma and Saltelli (1996)]. In analogy to Eq. (28), it is

$$S_{x_i|z_j}^{\text{Sobol',T}} = 1 - \frac{\text{Var}_{x_{\sim i}}[E[z_j|x_{\sim i}]]}{\text{Var}[z_j]}. \quad (29)$$

The subscript $x_{\sim i}$ indicates the consideration of all input quantities $x_k \mid k = \{1, \dots, n_x\}$ holding $k \neq i$. Conclusively, $\text{Var}_{x_{\sim i}}[E[z_j|x_{\sim i}]]$ is the partial variance of all input quantities x_k without x_i .

Coefficient of Prognosis – CoP The sensitivity measure Coefficient of Prognosis is defined in Most et al. [Most and Will (2011)] as

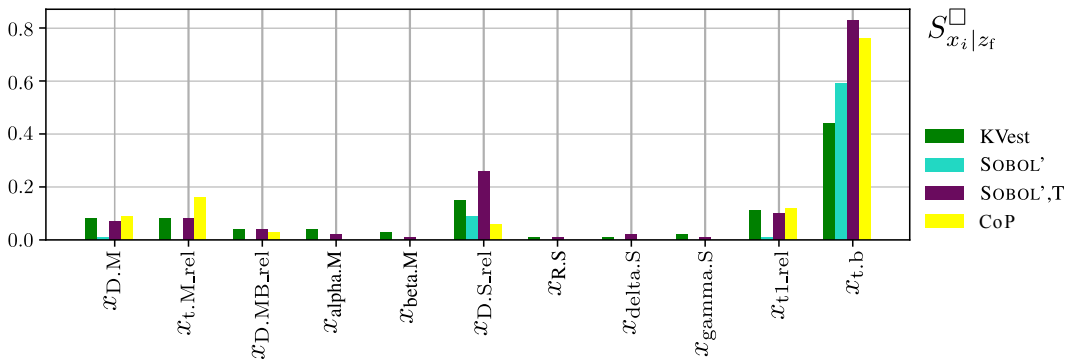
$$S_{x_i|z_j}^{\text{CoP}} = CoP_{z_j} \cdot S_{x_i|z}^{\text{Sobol',T}}. \quad (30)$$

The measure is the total SOBOL' index linearly scaled by the Coefficient of Prognosis, which is a quality estimator for the meta-model. The quality estimators CoP of the polynomial approximation for the two results are $CoP_{z_f} = 0.9169$ and $CoP_{z_{t,n}} = 0.9866$.

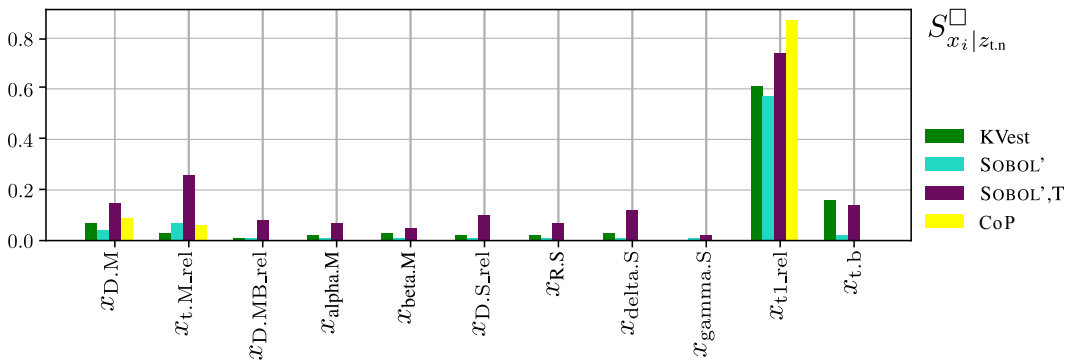
5.2 Results of sensitivity analysis based on meta-model computations

Additionally to the above described measures, the measure KWest, already discussed in Section 3.2, is included in the comparison. The computed sensitivities can be found in Figs. 17(a) and 17(b) for the response interlock z_f and neck thickness $z_{t,n}$, respectively.

KWest versus SOBOL' As already pointed out in Section 3.2, the sensitivity measure KWest is comparable to SOBOL' indices of first order. But, in this example there is a substantial difference between them. The measure KWest identifies more sensitive parameters than the SOBOL'-indices. Only the most significant parameters are found by both. One reason for the difference is the dependency of the input data, see Figs. 6 and 8 and Eqs. (8) and (11). Within the sampling-based sensitivity measures, the dependencies cannot be considered and cause the differences. Another reason of difference is the usage of the meta-model for computing the SOBOL' indices. To capture such influences, sensitivity measures based on existing data and sampling-based measures need to be compared.



(a) Sensitivities for z_f (interlock)



(b) Sensitivities for $z_{t,n}$ (neck thickness)

Figure 17: Sampling-based and existing data-based sensitivity measures

SOBOL' versus SOBOL',T The comparison of the total SOBOL' indices and the first order indices indicates the amount of interaction phenomena. For the both result quantities, a huge difference can be found. For z_f , the parameters $x_{D.S_rel}$ and x_{t1_rel} are different. For $z_{t,n}$, many parameters show interaction phenomena, but especially $x_{t.M_rel}$, x_{t1_rel} and $x_{t.b}$ need to be highlighted.

SOBOL',T versus CoP The comparison yields, that the selection of the type of meta-model has a significant influence on the sensitivity evaluation. The measure CoP is a linear scaled total SOBOL' index, such that a comparison of the measures is possible. Even if the three most sensitive parameters (x_{t1_rel} , $x_{D.M}$, $x_{t.M_rel}$) for the result $z_{t,n}$ are identified with both measures, the differences are very substantial. The amount of influence and the interaction phenomena are very different.

5.3 Sectional sensitivities

Description of methodology In Pannier et al. [Pannier and Graf (2014)], a method for the sectional evaluation of global sensitivity measures is proposed. The aim is to have more detailed information about the sensitivity for x_i by separating the input space \mathbf{X} according to Eq. (1) into p equidistant intervals. The separation is done independently for each input parameter, such that the sensitivity is computed as function depending on x_i . The splitting is formulated as

$$\mathbf{X} = I_1 \times I_2 \times \dots \times \bigcup_{k=1}^p I_{i,k} \times \dots \times I_{n_x}, \quad (31)$$

$$\bigcup_{k=1}^p I_{i,k} = [a_{i,1}, b_{i,1}] \cup [a_{i,2}, b_{i,2}] \cup \dots \cup [a_{i,k}, b_{i,k}] \cup \dots \cup [a_{i,p}, b_{i,p}], \quad (32)$$

with $a_{i,k} = a_i + (k-1) \cdot \Delta$, $b_{i,k} = a_i + k \cdot \Delta$, $\Delta = \frac{b_i - a_i}{p}$. The same splitting is applied to the data set for the sensitivity measure ‘KVest’, see Eq. (13). For the input parameter x_i , all segments $\mathbf{X}_{i,k} = I_1 \times I_2 \times \dots \times I_{i,k} \times \dots \times I_{n_x}$ have to be considered. The sensitivity is computed for each segment of the input space $k \in \{1, \dots, p\}$, such that

$$S_{x_i,k|z_j}^{\square} = S_{x_i|z_j}^{\square}(\mathbf{X}_{i,k}) \quad (33)$$

is the sectional sensitivity for the input parameter x_i . As sensitivity measure, all common global sensitivity measures can be applied. For global comparison, these sectional sensitivities have to be scaled by

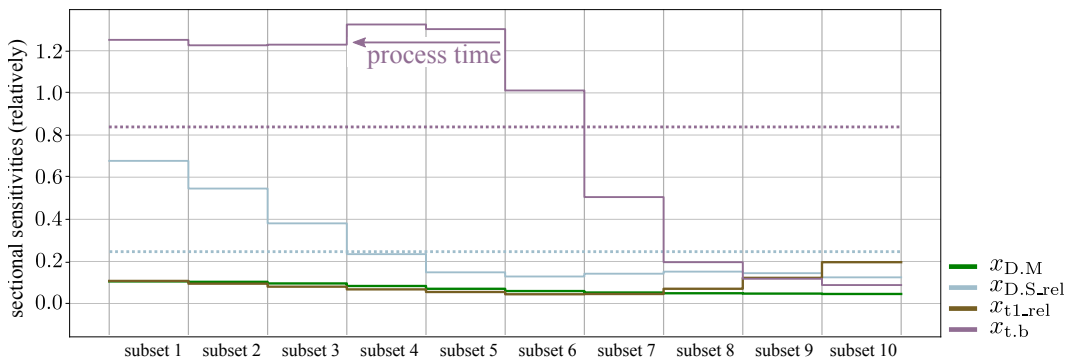
$$S_{x_i,k|z_j} = \frac{p \cdot S_{x_i,k|z_j}^{\square}}{\sum_{k=1}^p S_{x_i,k|z_j}^{\square}} \cdot S_{x_i|z_j} \quad (34)$$

Thus, the mean of the sectional sensitivity values is equal to the sensitivity of the full input space \mathbf{X} computed with the same global sensitivity measure S .

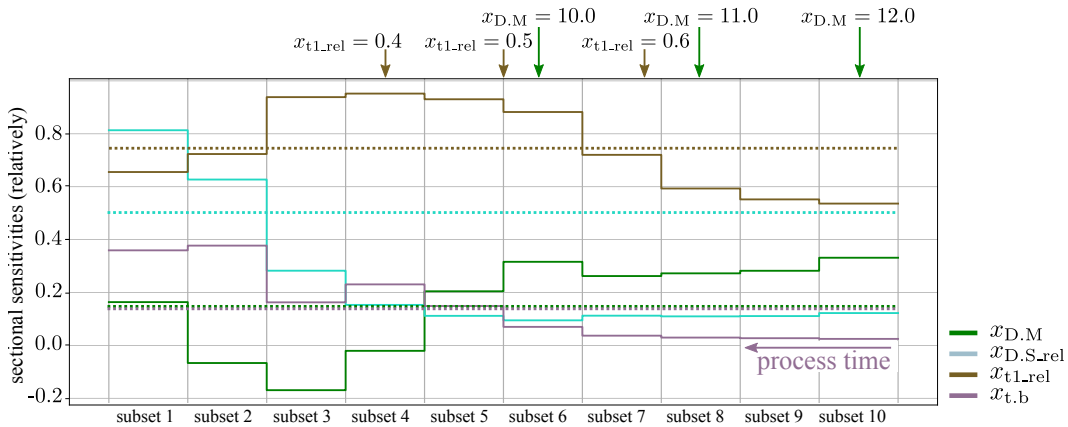
Sectional sensitivity can be interpreted as mean quantitative functional behaviour for each input parameter x_i under consideration of the variance of all others. For the interpretation of the results, it has to be considered, that the sensitivities between different input parameters are not comparable within one segment, because they are computed in different subspaces $\mathbf{X}_{i,k}$.

Results Here $p = 10$ sections are evaluated, the results are given in Fig. 18. Due to the high number of interaction phenomena, the total SOBOL’ index $S^{\text{Sobol’},T}$ is considered.

For the result z_f , the two parameters $x_{t,b}$ and x_{D,S_rel} are remarkable. All other parameters showing uniform behaviour, which means the influence is constant over the complete



(a) Sectional sensitivities for z_f (interlock)



(b) Sectional sensitivities for $z_{t,n}$ (neck thickness)

Figure 18: Selected sectional sensitivity using SOBOL',T (continuous lines) for 10 subsets and relevant original values (dashed lines, see Fig. 17)

input range. Furthermore, the dashed line in Fig. 18(a) (showing the result discussed in the previous section) is equal to the overall sensitivity. The parameter $x_{t,b}$ has very high sensitivity for low parameter values and lower sensitivity for high parameter values. This characteristic has to be evaluated according to the production process, low parameter values exist at the end of the process, see Fig. 1. To validate this result, the meta-model visualisation in Fig. 14(a) can be used. For small values of $x_{t,b}$, a very high gradient is observable. The same evaluation is valid for $x_{D,S,rel}$.

For result $z_{t,n}$, the input parameters $x_{t,rel}$, $x_{t,M,rel}$ and $x_{D,M}$ are significant. The parameter $x_{t,rel}$ is very sensitive and shows small changes only. The input parameter $x_{t,M,rel}$ shows decreasing sensitivity. This behaviour cannot be found in Fig. 15(a), presumably because the interaction sensitivity of $x_{t,M,rel}$ is very high, which cannot be visualized in a 3D-plot.

5.4 Summary of sensitivity results

The following main facts can be concluded:

- sensitivity of result z_f (interlock)
 - most relevant parameters: $x_{t,b}$ (bottom thickness), x_{D,S_rel} (punch diameter in relation to die diameter) and x_{t1_rel} (thickness upper sheet in relation to total sheet thickness),
 - same relevant parameters are found as on the basis of existing data, see Tab. 3,
 - parameter interaction exists in the meta-model,
 - sensitivity of $x_{t,b}$ (bottom thickness) decreases for high parameter values.
- sensitivity of result $z_{t,n}$ (neck thickness)
 - most relevant parameters: x_{t1_rel} (thickness upper sheet in relation to total sheet thickness), x_{t,M_rel} (die depth in relation to total sheet thickness), $x_{t,b}$ (bottom thickness) and $x_{D,M}$ (die diameter),
 - except x_{t,M_rel} , same relevant parameters are found as on the basis of existing data, see Tab. 3,
 - high amount of parameter interaction exists in the meta-model,
 - sensitivity of x_{t1_rel} (thickness upper sheet in relation to total sheet thickness) and x_{tM_rel} (die depth in relation to total sheet thickness) showing significant changes within the parameter range.
- dependency in the input data set does not allow to fully comparable the meta-model-based sensitivity measures and the sensitivities discussed in Section 3.2 (extrapolation of meta-model),
- results depend on the selected meta-model.

6 Decision map-engineering approach for visualisation of high-dimensional parameter spaces

A common engineering design approach is the visualisation of complex functional relationships by two-dimensional nomographs. These nomographs simplify the design process and helps to find appropriate parameter ranges for each problem. This approach is adapted for the ANN meta-model, developed in Section 4.2. The map should represent the 11-dimensional input vector \underline{x} , by two dimensions $\xi^{\text{map}}: \mathbb{R}^2 \rightarrow \mathbb{R}$. Thus, the function $\xi^*: \mathbb{R}^{11} \rightarrow \mathbb{R}$ needs to be constructed in a reduced way. In general, two methods can be used. First, by the application of dimension reduction methods, such as principal component analysis or singular value decomposition, the sample space can be reduced,

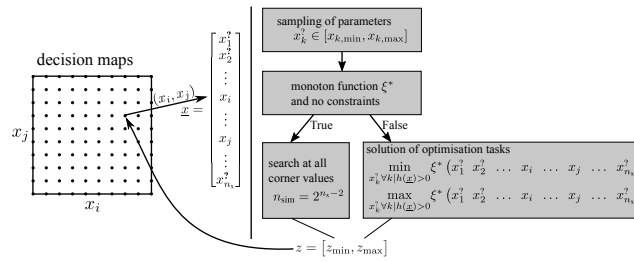


Figure 19: Proposed approach for generating decision maps

maybe to a two-dimensional space. Crucial is, that this space has no physical relationship and, therefore, engineering decisions cannot be made based on those values. The second methodology is proposed in this contribution and is based on the selection on two representative dimensions x_i, x_j , which are the map dimensions. The question to be answered is, what values should be taken for the others not shown parameters $x^?$. This aspect is previously already discussed for the meta-model visualisations in Figs. 14 and 15. The proposed method is to consider the not shown parameters $x^?$ as intervals and construct two decision maps. One decision map represents the lowest and the other the highest values. The computation of these extremal values needs to be repeated for each lattice point. In Fig. 19, the approach is shown, especially the consideration of constraints $h(\underline{x})$ is highlighted. The difference of the two maps can be interpreted as the influence of the not shown parameters $x^?$. It has to be remarked, that the common method plotting two signification input values and consider the others $x^?$ as mean value yields wrong interpretations.

6.1 Construction of decision maps for interlock and neck thickness

The major requirement for any design is permissibility. For the analysed sample set, no clear relationship of permissibility can be identified, see Fig. 6. To take this characteristic into account, the decision maps are built for the permissible design space, see Section 3.1. This hypercuboid Eq. (9) represents permissible samples only. Because of the interaction freedom of the hypercuboid with respect to the selection of samples, the maps can be made interaction free. Alternative approaches, as describing the permissible samples with the help of convex hulls, do not have this advantage.

For the functions $\xi^* = z_f$ and $\xi^* = z_{t,n}$, the monotony requirement cannot be guaranteed and two constraints need to hold. The constraints are due to the dependency of x_{t,M_rel} and x_{D,S_rel} , which can be seen in Fig. 6. The other identifiable dependencies, as x_{t1_rel} and $x_{t,b}$, are not present in the permissible design space. The constraints for permissibility are

formulated as

$$h_1(x) = x_{D,S_rel} - 0.50 \cdot x_{t,M_rel} - 0.50 < 0 \quad \text{and} \quad (35)$$

$$h_2(x) = x_{D,S_rel} - 0.32 \cdot x_{t,M_rel} - 0.43 > 0. \quad (36)$$

and $x_{D,M}$ are most sensitive in descending order. For the result $z_{t,n}$, the input parameter x_{t_rel} , x_{t,M_rel} and $x_{D,M}$ are most sensitive. The idea of the map is the visualisation the functional characteristics with respect to these input parameters. If only the two most sensitive parameters would be used, the resulting map would be too general and not applicable in practice. To overcome this, a grid of maps is computed, therefore fixed values of the third and fourth most sensitive parameters are considered. For z_f , no specific characteristic can be found in the sectional sensitivities, see Fig. 18(a). But, for $z_{t,n}$ the input parameter $x_{D,M}$ show a significant change in sensitivity, see Fig. 18(b). Therefore, the fixed values of the input parameter are placed in these regions, which are already indicated in Fig. 18(b). To directly include the constraints Eqs. (35) and (36), a link between z_f and $z_{t,n}$ is provided by sharing the parameter x_{D,S_rel} .

As depicted in Fig. 19, the values of the decision map should be represented by the minimum and the maximum $z = [z_{min}, z_{max}]$. If the optimisation tasks are solved, the extremal values are inside of extrapolation meta-model areas. This yields a drastic overestimation of the uncertainty and is not explainable in practice. To cope with this, the map is approximatively constructed by replacing the extremal values by empirical quantile values assuming $z_{min} \approx z_{0.01}$ and $z_{max} \approx z_{0.99}$. The random sampling of the input space is performed by Monte-Carlo simulation using a set of $n_{sim} = 50000$ samples for each lattice girder point.

The resulting maps for z_f and $z_{t,n}$ are shown in Figs. 21(a) and 21(b) for the minimum and maximum values, respectively.

The minimum maps can be used by the following steps, as indicated in Fig. 20:

1. define threshold for interlock
e.g. $z_f > 0.3$
→ region of permissible designs in maps for z_f and $z_{t,n}$ (green highlighted),
2. select permissible $x_{t,b}$ under consideration of a manufacturing constrain $x_{t,b} > 0.2 \cdot t.t$
e.g. $x_{t,b} = 1.0$,
3. select x_{D,S_rel} fulfilling objective $\max z_{t,n}$ and holding the constraints
e.g. $x_{D,S_rel} = 0.72$,
4. select x_{t,M_rel} fulfilling objective $\max z_{t,n}$ and holding the constraints
e.g. $x_{t,M_rel} = 0.53$.

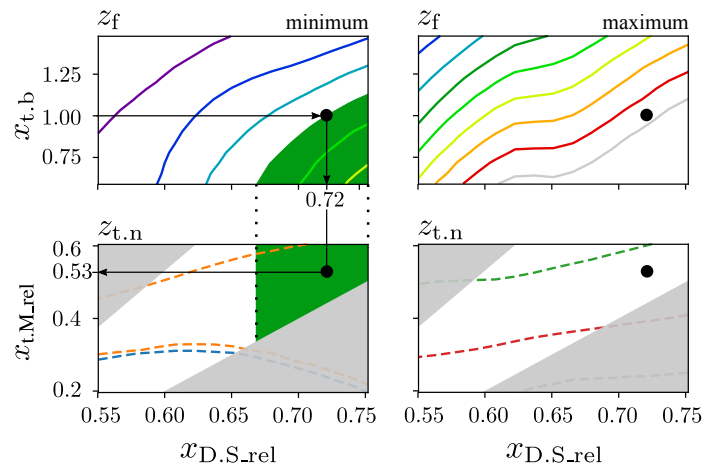


Figure 20: Example for using the decision map, with $x_{D.M} = 10.0$ and $x_{t1_rel} = 0.5$ (for colour legend see Fig. 21(a))

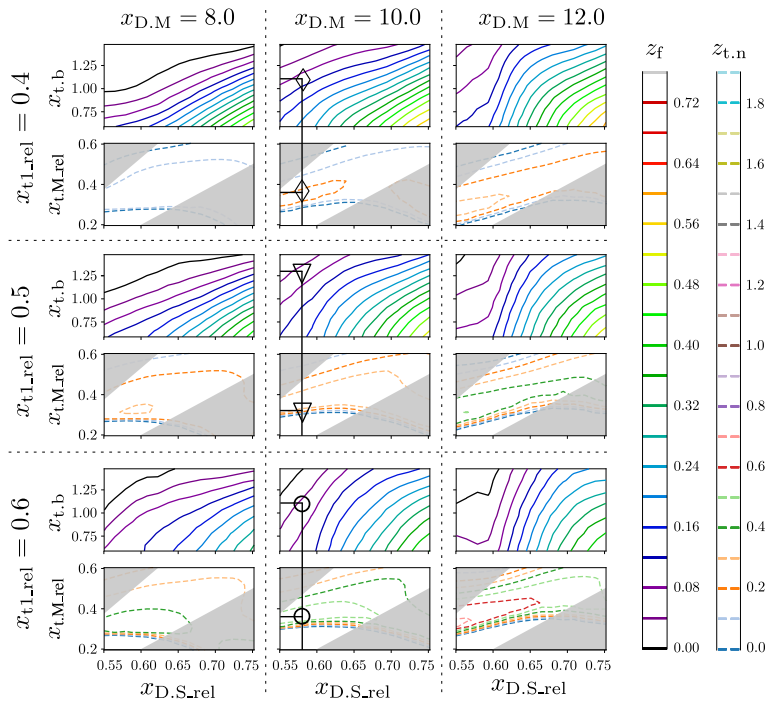
This results can be projected to the maximum map, yielding $z_f \in [0.34, 0.73]$ and $z_{t.n} \in [0.19, 0.44]$. For the further design process (finding the other parameters $x^?$), it is ensured, that the constraints hold and the result values are within the given intervals.

6.2 Evaluation of the decision maps

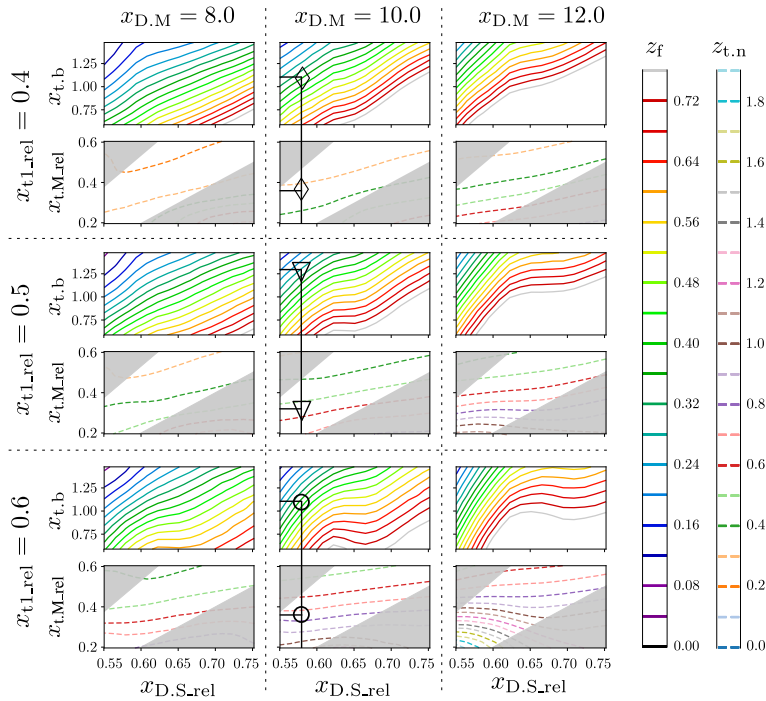
The evaluation of the decision maps (Figs. 21(a) and 21(b)) shows a significant difference between the minimum and the maximum value map. This shows the relevance of computing the extremal maps and not only a mean value map. A reason for the unexpected difference (unexpected because the most significant parameters are represented) can be the high amount of parameter interactions. This can be seen in Fig. 17 at the difference of first order SOBOL' index and the total SOBOL' index.

The minimum and the maximum maps for z_f show the same trend. Furthermore, it can be seen that for the three different $x_{D.M}$ a slight shift of the contour lines is recognisable. The change with respect to x_{t1_rel} depends on the value of $x_{D.M}$. The differences between the minimum and the maximum values are the same for all nine maps, which is indicated by, a shift of the contour lines for each and can be interpreted as nearly linear behaviour, w.r.t. $x_{D.M}$ and x_{t1_rel} . An important information of the sectional sensitivities (see Section 5.3) is, that the effect of high sensitivity in the first sections and less sensitivity in the last section for $x_{D.S.rel}$. This can also be found in the map, the gradient of the contour lines decreases for increasing $x_{D.S.rel}$. The same characteristic can be found for $x_{t.b}$.

The maps for $z_{t.n}$ are different compared to the maps for z_f . The shapes of the contour lines are different for the minimum and the maximum chart the uncertainty is higher. This means, for any selected design the range of possible values is higher. For the minimum map, the



(a) Minimum decision maps



(b) Maximum decision maps

Figure 21: Decision maps for z_f (interlock) and $z_{t,n}$ (neck thickness), with three testing points (\circ , \diamond , ∇) and highlighted constraints (see Eqs. (35) and (36))

change is more significant. The change with respect to $x_{t,b}$ is negligible. In comparison to the sensitivities (see Section 5.2), it can be seen, that the influence of x_{t1_rel} is higher than for x_{t,M_rel} . But x_{t,M_rel} has significant influence to the minimum map.

6.3 Application of decision maps for real test specimens

To show the applicability of the decision maps and evaluate their quality, three specimens are simulated and tested. In Tab. 4, the input parameters and the results are given. The photography of the real test specimens 2.1 is given in Fig. 2.

It can be seen, that the meta-model results for the neck thickness $z_{t,n}$ are very accurate and less accurate for the interlock z_f . The results applying the maps are also given in Figs. 21(a) and 21(b). The evaluation of the map indicates a range of possible responses due to the limited information content in two-dimensions. It is obvious that the expected results for the neck thickness $z_{t,n}$ are in the ranges of the maps. The prediction quality of the map for the interlock z_f is less, but suitable. The validity of the decision maps depends on the approximation quality of the meta-model, which can clearly be seen from the table. For more detailed maps, construction of an improved meta-model, e.g. only within the permissible range is suggested.

Table 4: Input and response parameters of three test specimens, related meta-model results z^* and results using the decision maps z^{map}

parameter	specimen 2.1 \circ	specimen 2.2 \diamond	specimen 2.3 ∇
$x_{D,M}$	10.0	10.0	10.0
x_{t,M_rel}	0.36	0.36	0.32
x_{D,S_rel}	0.58	0.58	0.58
x_{t1_rel}	0.6	0.4	0.5
$x_{t,b}$	1.1	1.1	1.3
z_f	0.31	0.46	0.30
z_f^*	0.27	0.33	0.22
z_f^{map}	[0.05, 0.36]	[0.10, 0.36]	[0.06, 0.28]
$z_{t,n}$	0.69	0.27	0.47
$z_{t,n}^*$	0.60	0.26	0.44
$z_{t,n}^{map}$	[0.05, 0.75]	[0.20, 0.33]	[0.25, 0.55]

Remark to the term ‘uncertainty’ *In general, the term uncertainty has multiple usages. In this contribution, it is used to indicate the unknown information due to the dimension reduction for the visualisation purposes. This kind of uncertainty can be seen within the context of early stage of design. The second main usage of the term uncertainty is in context of imprecisely known model parameter for a particular design, which is not in the scope of this contribution.*

7 Conclusion

The contribution comprises the evaluation and determination of information based on numerical simulations of the physical joining process of two metal sheets (clinchng). Accurate numerical simulations are inevitable since related physical experiments tend to be economically and ecologically expensive compared to the numerical pendant. Therefore, multiple simulations are utilized to obtain overall knowledge related to the clinching process. Based on the computed simulation results data mining methods, correlation and sensitivity analysis could be applied, gaining general insight to the manufacturing process with respect to inherent system interdependencies. The utilized methods are briefly introduced and discussed regarding their applicability. Basically, the applied correlation and sensitivity measures indicate the same set of input parameters as either dependent to each other or sensitive to particular output dimension.

As usual in engineering related design process, it is helpful to provide design guidelines. Since the single evaluation of a certain design by a numerical simulation is highly computational expensive, an approach for a meta-model-based guideline has been created. By substituting the design space by an artificial neural network, it is possible to validate the data-based sensitivity and correlation indices, whereas it is worth mentioning, that the approximation quality strongly dependence on the non-linearity of the output parameters. Additionally, the determination of sectional sensitivity is carried out, which allows the computation of sensitivities in subsets of the input space and, therefore, process related changes of influence. The combination of the meta-model and data mining results lead to so-called decision maps, representing the point-wise evaluated meta-model over the most sensitive parameters. This 2D-representation of the clinching process enables the prediction of an initial design based on output requirements. As shown in the contribution, the utilization of mean values for input parameters could be misleading, wherefore extremal value are used. The generated decision has been exemplary validated.

Conclusively, the application of data mining methods in combination with the meta-model approximation enables a gain in process insight and simultaneously a visualisation of the clinching process provided by the decision maps. Nevertheless, the evaluation and application strongly dependence on the initial data set and its completeness regarding the representation of the mechanical/physical process.

Acknowledgement: This research is financially supported by the Deutsche Forschungsgemeinschaft (DFG) under grants GR 1504/9, KA 1163/34 and by the DFG Priority Programme ‘Polymorphic uncertainty modelling for the numerical design of structures – SPP 1886’ under grants GR 1504/11, KA 1163/37. The support of the DFG is gratefully acknowledged. Furthermore, the project P1172 of the ‘Forschungsvereinigung Stahlanwendung e.V. (FOSTA)’ is gratefully acknowledged for providing the clinching data.

References

- Arlot, S.; Celisse, A.** (2010): A survey of cross-validation procedures for model selection. *Statistics Surveys*, vol. 4, pp. 40-79.
- Breunig, M. M.; Kriegel, H. P.; Ng, R. T.; Sander, J.** (2000): Lof: Identifying density-based local outliers. *Proceedings of International Conference on Management of Data (ACM SIGMOD)*, pp. 93-104, Dallas.
- Chang, C.-C.; Lin, C.-J.** (2011): Libsvm: A library for support vector machines. *ACM Transactions on Intelligent Systems and Technology*, vol. 27, pp. 1-27.
- Cherkassky, V.; Ma, Y.** (2004): Practical selection of svm parameters and noise estimation for svm regression. *Neural Networks*, vol. 17, no. 1, pp. 113-126.
- Dubourg, V.** (2011): *Adaptive Surrogate Models for Reliability Analysis and Reliability-Based Design Optimization (Ph.D. Thesis)*. Université Blaise Pascal, Clermont-Ferrand.
- Duddeck, F.; Wehrle, E.** (2015): Recent advances on surrogate modeling for robustness assessment of structures with respect to crashworthiness requirements. *10th European LS-DYNA Conference*, Würzburg.
- Geisser, S.** (1975): The predictive sample reuse method with applications. *Journal of the American Statistical Association*, vol. 70, pp. 320-328.
- Götz, M.; Liebscher, M.; Graf, W.** (2012): Efficient detection of permissible design spaces in an early design stage. *11. LS-DYNA Anwenderforum*, Ulm.
- Graf, W.; Götz, M.; Kaliske, M.** (2018): Computing permissible design spaces under consideration of functional responses. *Advances in Engineering Software*, vol. 117, pp. 95-106.
- Hagan, M. T.; Menhaj, M. B.** (1994): Training feedforward networks with the marquardt algorithm. *IEEE Transactions on Neural Networks*, vol. 5, pp. 989-993.
- Halkidi, M.; Batistakis, Y.; Vazirgiannis, M.** (2001): On clustering validation techniques. *Journal of Intelligent Information Systems*, vol. 17, pp. 107-145.
- Homma, T.; Saltelli, A.** (1996): Importance measures in global sensitivity analysis of nonlinear models. *Reliability Engineering and System Safety*, vol. 52, pp. 1-17.
- Inselberg, A.** (1985): The plane with parallel coordinates. *The Visual Computer*, vol. 1, pp. 69-91.
- Jin, R.; Chen, W.; Simpson, T. W.** (2001): Comparative studies of metamodelling techniques under multiple modelling criteria. *Structural and Multidisciplinary Optimization*, vol. 23, pp. 1-13.
- Landgrebe, D.; Kropp, T.; Gehrke, J.; Schön, A.; Ungemach, D.; Kleemann, G.** (2017): Mechanisch gefügte Stahlstrukturen in Fahrzeugbau und Bauwesen. *Europäische Forschungsgesellschaft für Blechverarbeitung e.V.: Gemeinsame Forschung in der Mechanischen Fügetechnik*, pp. 107-113.

- Landgrebe, D.; Mauermann, R.; Kropp, T.** (2017): Clinching-an innovative joining technology for trucks. *5th International Conference on Steels in Cars and Trucks*, SCT.
- Levenberg, K.** (1944): A method for the solution of certain no-linear problems in least squares. *Quarterly of Applied Mathematics*, vol. 2, pp. 164-168.
- Liebscher, M.; Witowski, K.; Goel, T.** (2009): Decision making in multi-objective optimization for industrial applications - data mining and visualization of pareto data. *8th World Congress on Structural and Multidisciplinary Optimization*, Lisbon.
- Malone, J.; McGarry, K.; Wermter, S.; Bowerman, C.** (2005): Data mining using rule extraction from kohonen self-organising maps. *Neural Computing and Applications*, vol. 15, pp. 9-17.
- Marquardt, D. W.** (1963): An algorithm for least-squares estimation of nonlinear parameters. *Society for Industrial and Applied Mathematics*, vol. 11, pp. 431-441.
- McKay, M. D.; Conover, W. J.; Beckmann, R. J.** (1979): A comparison of three methods for selecting values of input variables in the analysis of output from a computer code. *Technometrics*, vol. 21, pp. 239-245.
- Most, T.; Will, J.** (2010): Recent advances in metamodel of optimal prognosis. *Weimar Optimization and Stochastic Days*.
- Most, T.; Will, J.** (2011): Sensitivity analysis using the metamodel of optimal prognosis. *Weimar Optimization and Stochastic Days*.
- Mostafa, M.** (2009): Shades of green: A psychographic segmentation of the green consumer in kuwait using self-organizing maps. *Expert Systems with Applications*, vol. 36, pp. 11030-11038.
- Myers, R. H.; Montgomery, D. C.; Anderson-Cook, C. M.** (2009): *Response Surface Methodology: Process and Product Optimization Using Designed Experiments*. Wiley, New York, 3 edition.
- OptiSLang** (2011): *The Optimizing Structural Language, An Users' Manual, version 3.2.1, Technical Report*. Dynardo GmbH, Weimar.
- Pannier, S.; Graf, W.** (2014): Sectional global sensitivity measures. *Reliability Engineering and System Safety*, vol. 134, pp. 110-117.
- Plischke, E.** (2010): An effective algorithm for computing global sensitivity indices (EASI). *Reliability Engineering and System Safety*, vol. 95, pp. 354-360.
- Saltelli, A.; Chan, K.; Scott, E. M.** (2008): *Sensitivity Analysis*. Wiley, New York.
- Saltelli, A.; Tarantola, S.; Chan, K. P.-S.** (1999): A quantitative model-independent method for global sensitivity analysis of model output. *Technometrics*, vol. 41, pp. 39-56.
- Siddique, N.; Adeli, H.** (2013): *Computational Intelligence: Synergies of Fuzzy Logic, Neural Networks and Evolutionary Computing*. Wiley, Chichester.
- Siebertz, K.; van Bebbber, D.; Hochkirchen, T.** (2010): *Statistische Versuchsplanung-Design of Experiments (DoE)*. Springer, Heidelberg.
- Simpson, T.; Poplinski, J.; Koch, P. N.; Allen, J.** (2001): Metamodels for computer-based engineering design: Survey and recommendations. *Engineering with Computers*, vol. 17, pp. 129-150.

- Sobol', I. M.** (1967): On the distribution of points in a cube and the approximate evaluation of integrals. *USSR Computational Mathematics and Mathematical Physics*, vol. 7, pp. 86-112.
- Sobol', I. M.** (2001): Global sensitivity indices for nonlinear mathematical models and their monte carlo estimates. *Mathematics and Computers in Simulation*, vol. 55, pp. 271-280.
- Sobol', I. M.; Kucherenko, S.** (2009): Derivative based global sensitivity measures and their link with global sensitivity indices. *Mathematics and Computers in Simulation*, vol. 79, pp. 3009-3017.
- Sudret, B.** (2008): Global sensitivity analysis using polynomial chaos expansions. *Reliability Engineering and System Safety*, vol. 93, pp. 964-979.
- Ultsch, A.** (2003): Maps for the visualization of high-dimensional data spaces. *Technical Report*, DataBionics Research Lab, Universität Marburg.
- Wilson, D. R.; Martinez, T. R.** (2003): The general inefficiency of batch training for gradient descent learning. *Neural Networks*, vol. 16, pp. 1429-1451.
- Zimmermann, M.; von Hoessle, J. E.** (2013): Computing solution spaces for robust design. *Numerical Methods in Engineering*, vol. 94, pp. 290-307.